Journal of Nuclear Materials 394 (2009) 174–181

Contents lists available at ScienceDirect

Journal of Nuclear Materials

journal homepage: www.elsevier.com/locate/jnucmat

Atomic and dislocation dynamics simulations of plastic deformation in reactor pressure vessel steel

Ghiath Monnet [a,*], Christophe Domain [a], Sylvain Queyreau [a], Sanae Naamane [a], Benoit Devincre [b]

[a] EDF-R&D, MMC, Avenue des Renardières, 77818 Moret sur Loing, France
[b] LEM, CNRS-ONERA, 29 av. de la division Leclerc, 92130 Chatillon, France

A B S T R A C T

The collective behavior of dislocations in reactor pressure vessel (RPV) steel involves dislocation properties on different phenomenological scales. In the multiscale approach, adopted in this work, we use atomic simulations to provide input data for larger scale simulations. We show in this paper how first-principles calculations can be used to describe the Peierls potential of screw dislocations, allowing for the validation of the empirical interatomic potential used in molecular dynamics simulations. The latter are used to compute the velocity of dislocations as a function of the applied stress and the temperature. The mobility laws obtained in this way are employed in dislocation dynamics simulations in order to predict properties of plastic flow, namely dislocation–dislocation interactions and dislocation interactions with carbides at low and high temperature.

1. Introduction

In this paper we report on the dislocation behavior in the reactor pressure vessel (RPV) steel. Results are obtained using a multiscale modeling approach and were obtained in the framework of the European project PERFECT (FI60-CT-2003-208840). Dislocation properties and interactions are investigated on two phenomenological scales, the atomic and the continuum (mesoscopic) levels. Atomic simulations using first principles and molecular dynamics (MD) techniques are used for a direct investigation of dislocations, taking into account the dislocation core structure in iron and its related thermally activated processes. We explain how atomic simulation results can be used to provide a continuous description that allows for the identification of mesoscopic quantities. Dislocation dynamics (DD) simulations are then used to study dislocation properties including mobility, dislocation–dislocation interactions and modeling of the Orowan process at low and high temperature.

2. Atomic simulation study of the screw dislocation properties at low temperature

In iron and at low temperature, the flow stress is strongly temperature dependent. The dislocation microstructure of strained specimens is basically formed of long and straight screw segments [1]. This dislocation microstructure is a direct consequence of the anisotropy of the dislocation mobility. Screw dislocations move much slower than non-screw dislocations [2–4]. The mobility of screw segments is therefore expected to control plastic flow in iron. The motion of screw dislocations occurs through the nucleation and the propagation of kink-pairs (KPs) along their lines. The KP mechanism is a thermally activated process, which explains the strong temperature dependency of the flow stress in iron. In this context, first-principles (ab initio) calculations, molecular statics (MS) and molecular dynamics (MD) simulations are of first interest to study the dynamical response of screw dislocations in iron submitted to a pure shear load at 0 K and at finite temperature). Parts of the results reported in this section have already been published elsewhere. Here we recall some of these results and show more recent results obtained with ab initio calculations.

2.1. Simulation techniques

Ab initio simulations are carried out using the conjugate gradient algorithm except for the outer atomic shell, which was fixed. These calculations were performed using the VASP code [5,6] and a 75 atom supercell. The projector augmented wave pseudopotential [7] taken from the VASP library was used within the spin polarized generalized gradient approximation. For the study of the dislocation motion at 0 K and finite temperature, MS and MD simulations were also used. The latter calculations were performed at constant strain rate. A screw dislocation is initially introduced at the center of the box. Periodic boundary conditions are applied in the direction parallel to the dislocation line. Four adjacent atomic planes are fixed in the upper and lower planes parallel to the

* Corresponding author. Tel.: +33 1 60 73 64 73; fax: +33 1 60 73 68 89.
E-mail address: ghiathmonnet@yahoo.fr (G. Monnet).

0022-3115/$ - see front matter © 2009 Elsevier B.V. All rights reserved.
doi:10.1016/j.jnucmat.2009.09.005

($\bar{1}10$) surfaces. The shear stress is calculated on the fixed atoms from the force component parallel to the Burgers vector b.

2.2. Ab initio and MS simulation results

A crucial point for the atomic calculations is the empirical atomic potential used. The embedded atom method (EAM) potential developed by Ackland et al. [8] was found to predict a core structure with a threefold symmetry for the screw dislocation in disagreement with ab initio results [9]. In our case, we use the recent potential developed by Mendelev et al. [10]. In ab initio, the core is compact with no preferential spreading, as well as in Ta, Wor Mo [11,12]. The Mendelev potential was the first one that leads to almost the same core structure as predicted from ab initio calculations, see Fig. 1. We use the [1 1 1] projection of the atomic positions to display the core structure. In this projection, the positions form a succession of triangles. The center of gravity of the dislocation may belong to one of these triangles.

Applying a shear on the ($\bar{1}10$) surface parallel to the dislocation line in ab initio and in MD simulation boxes generates a mechanical force on the screw dislocation and leads to a translation of the whole dislocation line. During the load, the core is deformed and moves in the [1 1 1] projection of the simulation cell (see Fig. 2) from one triangle to the other. In Fig. 2, we show the evolution under load of the core structure obtained by both ab initio and MS simulation using the Mendelev potential.

From this figure, it is easy to see that the structure of the dislocation core is modified depending on the nature of the triangle (soft or hard). But the main point here is that the configuration in the hard triangle (Fig. 2b) is found to be a metastable position for the dislocation. The reason is that when the dislocation reaches this position, it remains until an additional shear of the simulation box is applied. This means that the corresponding core structure is the stable configuration of the core in the hard triangle. In order to push the dislocation out of this position, a significant stress is needed. In other words, this position corresponds to a local minimum of the system energy during the dislocation displacement. This result was obtained using both first principle (VASP) calculations and MS simulation using the Mendelev potential. All the calculations reproduce the same displacement of the dislocation core and reveal the same metastable position. This result disagrees with the calculations made by Ventelon and Villaime [13], where no metastable position was found. The origin of this disagreement is not clear for the authors. We expect the difference in boundary conditions to be the reason. In addition, dislocation core displacement is found to occur completely on the ($\bar{1}10$) plane in agreement with experiment [14,15] and with the preferred slip plane for the formation of KPs found in MD simulations.

2.3. MD simulation results

In all MD simulations, motion of the screw dislocation occurs through the nucleation and the propagation of KPs along the dislocation line, as shown in the scheme of Fig. 3.

A KP nucleation corresponds to a jump of the dislocation to an adjacent triangle (in the [1 1 1] projection). Our results show that every KP process is systematically and quickly followed by another KP nucleation. Hence, the dislocation passes to a second adjacent triangle. The reason is that a single KP moves the dislocation from a "soft" triangle, with low core energy, to "hard" triangle, with higher core energy. The latter position is metastable; thermal activation allows the dislocation to pass rapidly to the next stable position and recover its core configuration in the soft triangle. The critical stress (T_c) for dislocation displacements in our MD simulations is found to be a function of two independent parameters: the applied velocity v and the absolute T. T_c is found substantially larger than the critical stress found in experiment. However, it was shown that it is possible to explain such difference by comparing the different parameters involved in the thermal activation process, i.e. the dislocation length and the effective velocity. The dislocation length and velocity are, respectively, in the order of magnitude of 1 μm and 1 μm/s in experiment, while they are close to 10 nm and 4 m/s in MD simulations.

3. Dislocation collective behavior in the RPV steel

Ultimately, a crystalline plasticity law designed for bainite should account for three characteristic features of the RPV steel microstructure: (i) a large initial dislocation density, (ii) a large friction stress and (iii) the existence of a carbide distribution. To each one of these features, special DD calculations were dedicated. In this section we summarize the corresponding results and effects on the flow stress. It must be noted that the three different features under investigation are not independent. For example, the presence of carbide may, in principle, decrease the slip systems interaction coefficients [16]. The contribution of the bainitic morphology to the mechanical response cannot be taken into account for instance owing to the specific characteristics of the grain boundaries. It is obviously necessary to validate a crystalline plasticity law first through prediction of the mechanical behavior of single crystals.

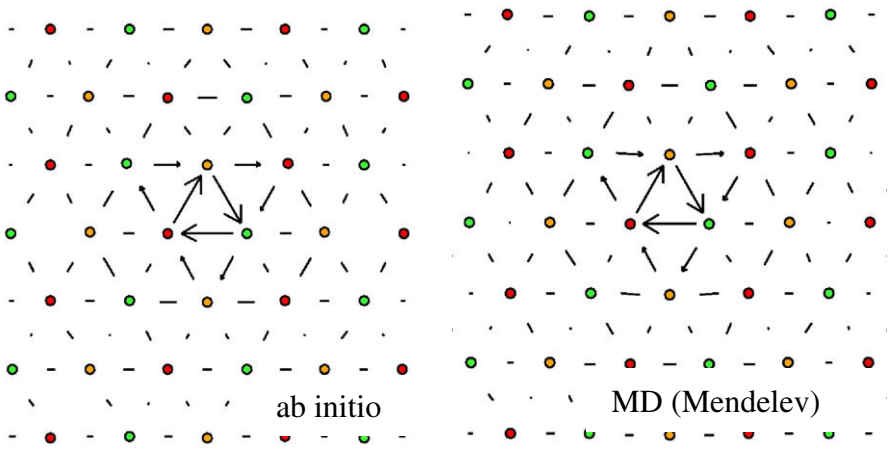

Fig. 1. The [1 1 1] projection of the crystal showing the core structure of the screw dislocation obtained by first principle calculations (ab initio) and molecular static (MS) using the Mendelev potential.

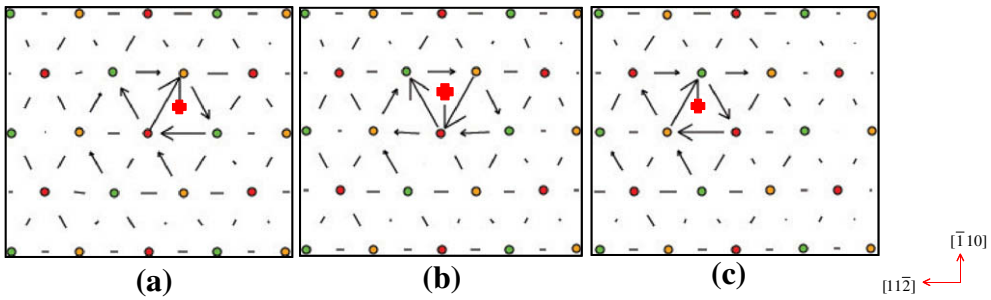

Fig. 2. Ab initio simulations of the rigid displacement (from (a) to (c)) of the dislocation core under a shear strain applied in the [1 1 1] direction, perpendicular to the figure.

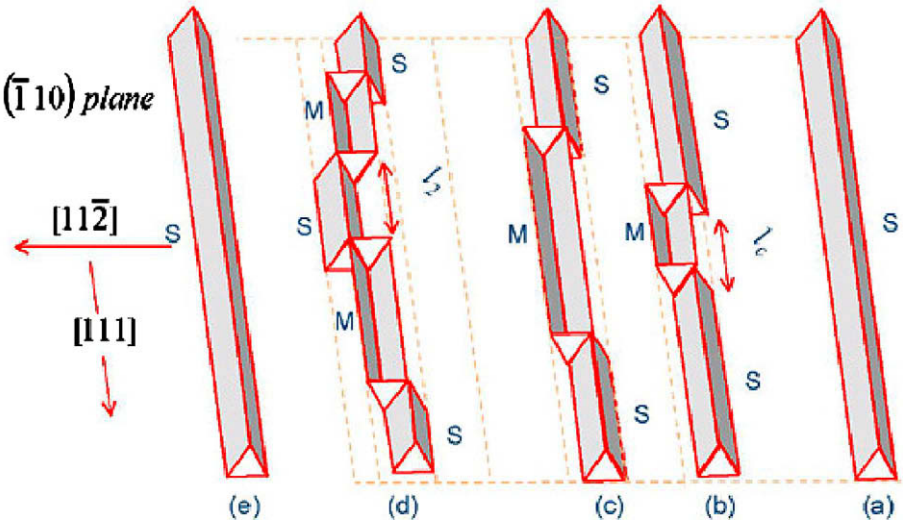

Fig. 3. A scheme showing the mechanism of motion of the screw dislocation. S and M denotes the stable and metastable dislocation positions in the soft and hard triangles.

Only when this validation is achieved can the role of a boundary be investigated.

3.1. Mobility laws of dislocations

The nature of the dislocation mobility law in bcc materials depends on the temperature and dislocation character. At room and high temperature, the mobility of all dislocations of all characters looks like the one observed in fcc crystals, hence can be described with a simple viscous law. But at low temperature, the screw dislocation mobility decreases drastically and therefore the above approximation is not correct.

At low temperature the mobility law, that allows the velocity of a screw segment v_{screw} to be deduced as a function of the effective stress τ^*, was fitted to experimental results using a formula proposed by Kocks et al. [17]. Results of such fitting, in agreement with MD simulations, provides the following equation:

$$v_{\text{screw}} = H\,L\,\exp\left(-\frac{\Delta H_0}{kT}\right)\,2\,\sin h\left(\frac{\Delta H_0}{kT}\sqrt{\frac{\tau^*}{\tau_0}}\right), \tag{1}$$

where H and τ_0 are constant, L the screw segment length and ΔH_0 the total activation energy close to 0.84 eV. The value of is τ_0 is 363 MPa and should not be confused with the critical stress at 0 K, but the result of a fitting process.

Concerning edge dislocations, very little experimental information about their mobility at low temperature is available. Characterization using MD simulation was only performed in pure iron and the corresponding viscous drag coefficient is not appropriate in the case of RPV steel. This is why, an assumption is made that the mobility of edge dislocation is only proportional to that of screw dislocations with a factor K much larger than unity. Explicitly, the velocity of edge segment is given by

$$v_{\text{edge}} = v_0 K \exp\left(-\frac{\Delta H_0}{kT}\right)\,2\,\sin h\left(\frac{\Delta H_0}{kT}\sqrt{\frac{\tau^*}{\tau_0}}\right), \tag{2}$$

where v_0 is constant and taken equal to 10^5 μm/s. The factor K is a strongly decreasing function of temperature. The values of K taken in our simulations are: 10^6, 10^4, 10^3, 200, and 50 at the investigated temperatures: 50, 100, 150, 200, 250 K. This simple phenomenological solution ensures that the difference in mobility between screw and non-screw segments decreases with temperature in agreement with experience.

3.2. Dislocation microstructure in RPV steel

Few observations were reported in the literature concerning dislocation distribution in RPV steels. However, two investigations were performed recently to describe the microstructure of non-deformed and plastically deformed RPV steel [18,19]. The results indicate that RPV steel is characterized by a large dislocation density, close to $10^{14}\,\text{m}^{-2}$. Since interaction coefficients measured according to the Franciosi model [20,21] depend on the dislocation density [22,23], they were evaluated again, on the basis of the following formula [24] and using a large density of forest dislocations, fixed to $10^{13}\,\text{m}^{-2}$ per slip system.

$$\tau_c^p = \mu b\sqrt{\sum_s\left[\frac{\ln\left(1/b\sqrt{\beta^{ps}\rho^s}\right)}{\ln\left(1/b\sqrt{\beta^{ps}\rho_{\text{ref}}}\right)}\right]\beta^{ps}\rho^s} + \tau_F, \tag{3}$$

where τ_c^p is the critical stress on system "p", ρ^s the density of dislocations belonging to system "s", ρ_{ref} the reference density used to evaluate the interaction coefficient, typically of the order of 10^{13} m^{-2}. β ps denotes here the interaction coefficient between system "s" and "p", and τ_F the friction stress corresponding to the solid solution strengthening (see next section). The interaction coefficients are calculated with the help of DD simulations of latent hardening. Although, several parameters needed in DD simulations may affect results, their influence was not reported in [25]. Studies of sensitivity to these parameters were therefore carried out within physically accepted ranges. Here we present results of two studies: the strain rate effect and the role of the length of the Frank-Read sources used to introduce forest dislocations (Fig. 4). It is shown that the computed value of β does not depend on the strain rate when the latter varies between 1000 and 8000 s^{-1}. Although, these values seem large compared with experiment (in the order of 10^{-4} s^{-1}), the associated dislocation velocities are quite reasonable. The reason is that the strain rate is proportional to the mobile dislocation density when the velocity of dislocations is kept constant. Since the dislocation density was chosen relatively large in the simulation in order to reproduce the RPV microstructure, on can perform DD simulations with large fixed strain rate. The average dislocation velocity in our simulations is found in the order of some m/s.

On the other hand, the dependency of the interaction coefficients on the size of the forest segment length is pronounced if the latter is less than four times the average spacing between dislocations. Beyond this value, the interaction coefficient becomes insensitive to the length of the forest segments, see Fig. 4.

The results of the latent strengthening simulations are summarized in Table 1. Such interaction coefficient values are an important ingredient of a crystalline plasticity law for bainite.

In this table, we can clearly see that the collinear interaction is by far the strongest interaction, followed by the interaction leading to the formation of the mixed-symmetrical junction. Other junctions do not induce strong interactions.

3.3. Effect of the friction stress

A recent investigation reports the important role of alloy friction on the formation and the stability of dislocation junctions. It is thus important to estimate the alloy friction stress in bainite. In the case of RPV steel, interstitial carbon atoms are expected to provide the most important contribution to the solid solution strengthening. Unfortunately, carbon strengthening is difficult to estimate from experience. In Fig. 5a compilation of all available results reported in the literature on strengthening of carbon in iron solid solution is reproduced. In [26] we can find examples of tensile testes on pure iron single crystals. From this compilation and since the carbon content in RPV steel is close to 100 ppm wt. [27], we set the alloy friction value to 30 MPa in DD simulations [24].

DD simulations of latent strengthening were then repeated again using 30 MPa for the alloy friction and a second set of interaction coefficients was computed. The results, listed in Table 2, show no significant effect of the alloy friction, except, however, for the collinear interaction, which is still selected as the strongest interaction. The reason for such small sensitivity of the interaction coefficient on alloy friction is related to the large density of dislocations in RPV steel.

As pointed by Monnet and Devincre, the contribution of alloy friction to the interaction coefficients is significant only when the average dislocation spacing is larger than $R = \mu b/\tau_F$. In the case of the RPV steel, the average dislocation spacing is close to 100 nm

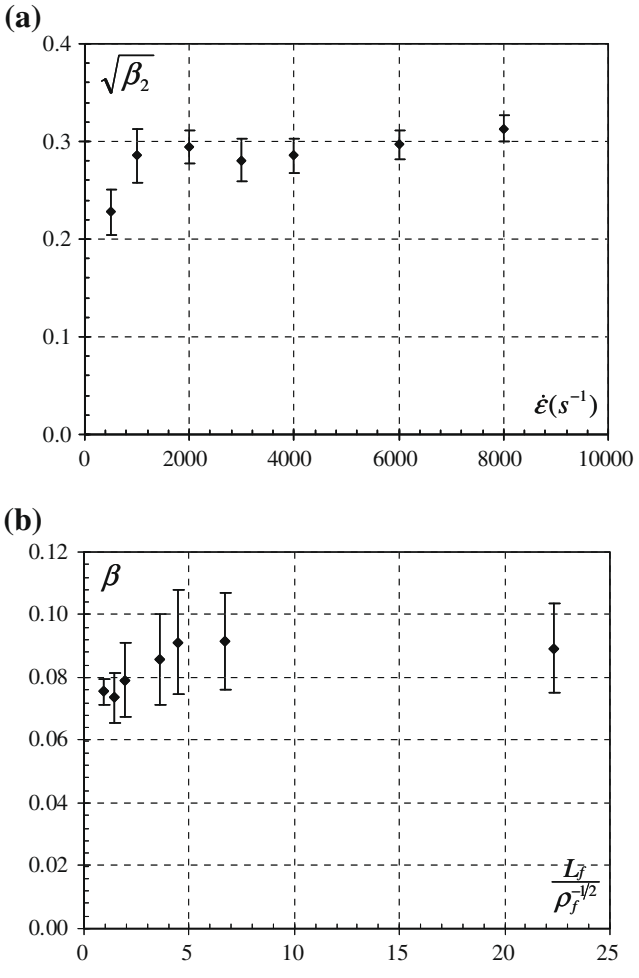

Fig. 4. Effect of (a) the strain rate and (b) the length of forest dislocations sources on the interaction coefficients, computed from DD simulations.

Table 1
Interaction coefficients determined by DD simulations.

Interaction nature	β_i (τ_F = 0 MPa)
1. Collinear interaction	0.704 ± 0.034
2. Mixed-symmetrical junction	0.098 ± 0.014
3. Mixed-asymmetrical junction	0.055 ± 0.009
4. Edge junction	0.062 ± 0.012

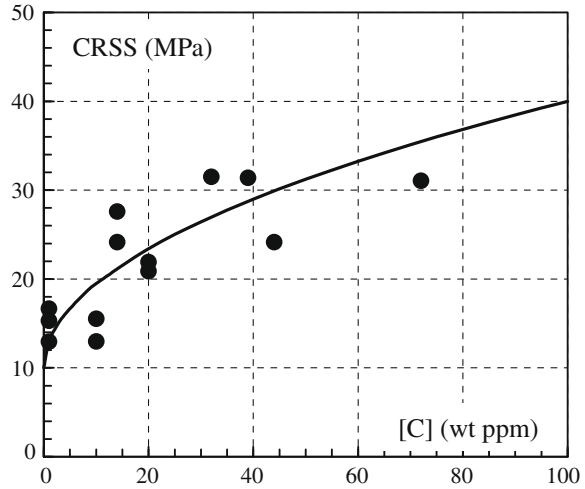

Fig. 5. Strengthening effect of carbon in solid solution of iron.

Table 2
Interaction coefficient computed with two different values of the alloy friction.

Interaction nature	β_i (τ_F = 30 MPa)	β_i (τ_F = 0 MPa)
1. Collinear interaction	0.536 ± 0.041	0.704 ± 0.034
2. Mixed-symmetrical junction	0.063 ± 0.006	0.074 ± 0.007
3. Mixed-asymmetrical junction	0.036 ± 0.006	0.040 ± 0.007
4. Edge junction	0.039 ± 0.005	0.042 ± 0.003

while the value of R is close to 600 nm. This is why alloy friction is expected to decrease the interaction coefficients only if $\tau_F > 200$ MPa. One can then conclude that alloy friction can hardly affect forest hardening, unless irradiation modifies strongly the solid solution composition.

4. Carbide strengthening

In RPV bainite, both inter-lath and intra-lath carbides were observed. These second phase precipitates are expected to strengthen the material owing to their size and distribution.

4.1. Carbide size and distribution

The major difficulty encountered here is precisely the determination of carbide size and spatial distribution. Indeed, RPV steel is a heterogeneous material. Experimental observations depend thus on the depth and/or size of the investigated volume. Few observations were reported in the literature [28], and most of them were dedicated to fracture investigation, where only large precipitates were characterized. If we consider only existing estimations one finds that the density of carbides is less than 10^{18} m^{-3} and therefore the strengthening induced by carbides must be negligible compared to forest hardening in RPV steel. To clarify this point, new investigations using a high resolution scanning microscope were made. Result of this characterization gave new insight of the carbide size and distribution, see Fig. 6.

Corresponding observations show an average size of carbides of approximately 100 nm and a number density close to 3×10^{19} m^{-3}. Hence, the corresponding average carbide spacing is in the same order of magnitude as the average dislocation spacing. For that reason, a strong carbide strengthening cannot be excluded and additional investigation was needed.

4.1.1. Accounting for the Orowan mechanism in DD simulation

Calculation of the carbide phase strengthening was performed using DD simulations following a method previously used for the investigation of irradiation-induced precipitation in zirconium alloys [29]. However, the initial computational method was modified. Every carbide was represented by a sphere of randomly distributed positions. The carbide shear resistance was modeled by a high friction stress to impose a penalty to dislocation dynamics inside the carbides. Since carbides are of large sizes and of incoherent structure, their shear resistance was set to infinity in a first step to simulate the Orowan mechanism.

4.1.2. Carbide strengthening at room and high temperature

In Fig. 7, we show the loading curve of a DD simulation box containing a dislocation density made of sources belonging to the primary slip system, with and without carbide distribution. Carbide strengthening effect is quite significant and this confirms that carbide strengthening is a competing process with forest strengthening. Moreover, simulations including carbides show a larger hardening rate when compared with the precipitate-free material. This result comes from the strong elastic interaction existing between mobile dislocations and the Orowan loops left around precipitates during plastic deformation.

This structural hardening can easily be compared to theoretical predictions made on the basis of an increase in the dislocation density with deformation. For this reason, the dislocation density was computed in DD simulations with and without carbides. In Fig. 8, we show evolution of the dislocation density as a function of plastic strain. From this figure it is clear that the Orowan mechanism increases dislocation storage rate by a factor of 50%.

Lastly, we can estimate from Fig. 7 the strengthening induced by carbide in RPV steel. It is of the order of 25 MPa. A forthcoming paper will be dedicated to the question of forest and carbide strengthening superposition.

4.2. DD simulations of carbide strengthening at low temperature

All models and theories on precipitation strengthening in the literature are based on the assumption that the dislocation mobility is independent of the segment character. Even the well-established model (called in the following the BKS model) proposed by Bacon et al. [30] cannot predict precipitation strengthening in non quasi-static conditions.

The mobility laws presented in Section 3.1 were checked to provide a good description of dislocation behavior at low temperature [31] and for that reason they were used in DD simulations to investigate carbide strengthening at low temperatures.

Given the complexity of the process, we started our investigation by studying the interaction of one infinite dislocation with an infinite periodic row of carbides. This allows us to determine

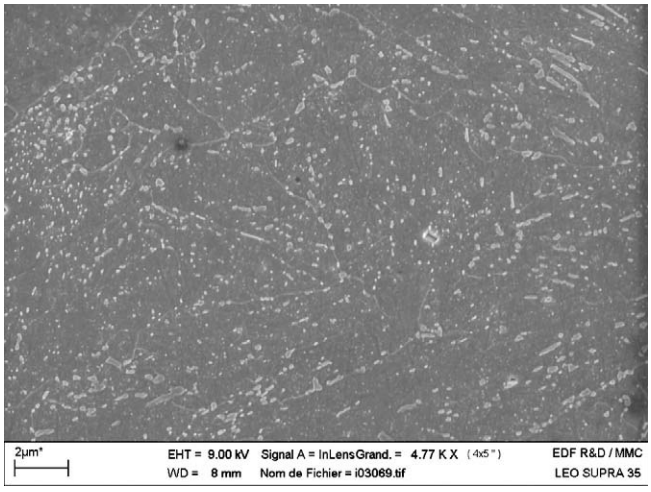

Fig. 6. Microstructure of RPV investigated using a high resolution scanning electron microscope.

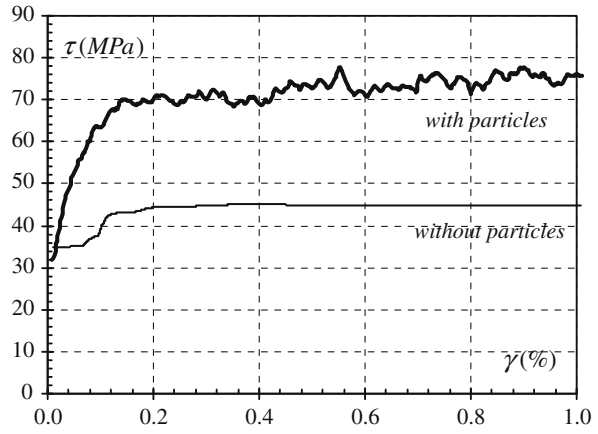

Fig. 7. Loading curve of the primary system with and without carbide distribution.

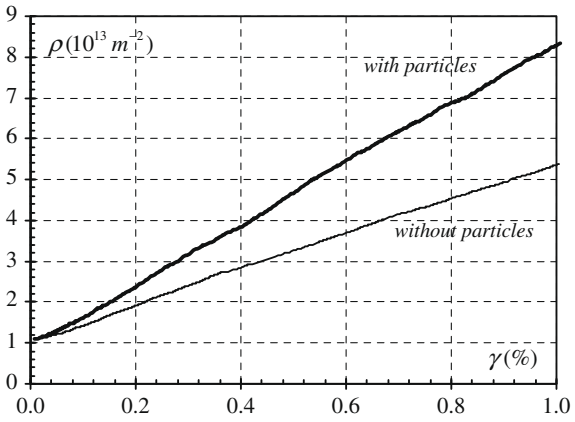

Fig. 8. Evolution of the dislocation density with and without carbide distribution.

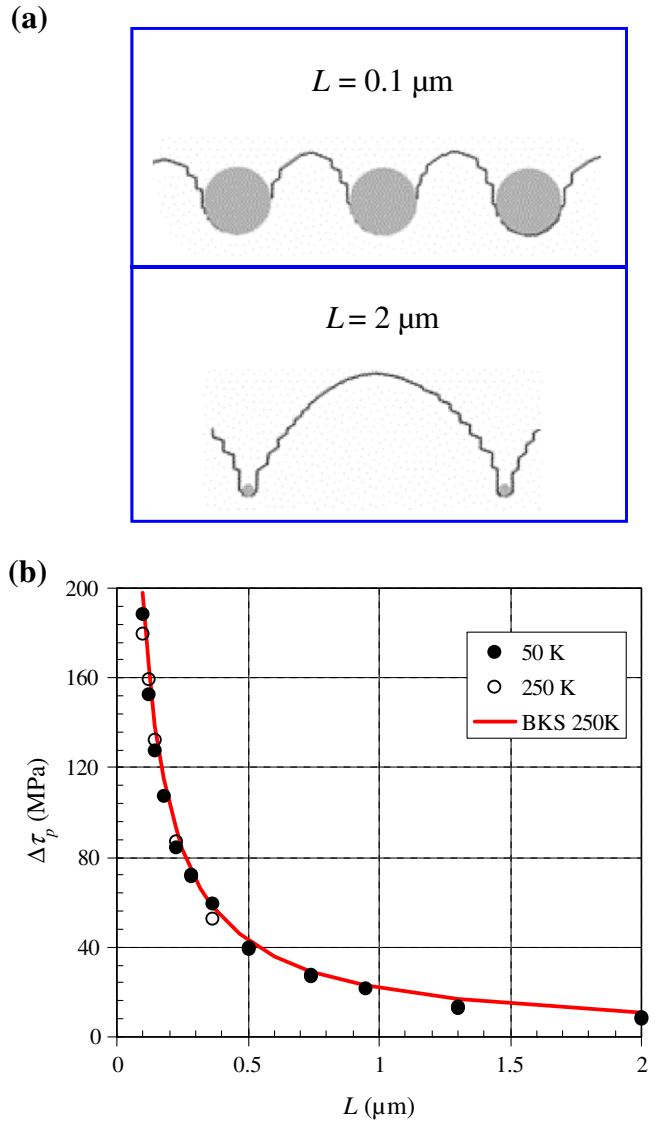

Fig. 9. (a) Critical shape of the edge dislocation at 50 K with different carbide spacing and (b) the Orowan strengthening as a function of carbide spacing for 50 and 250 K. The line recalls the prediction of the BKS model at 250 K.

the temperature and strain rate effects on the interaction. Then, in a second step, we studied the influence of more realistic carbide distribution on plastic flow.

4.2.1. Infinite edge dislocation interacting with periodic row of carbides

Although the edge dislocation mobility is temperature dependent, the length of dislocation segments does not affect their velocity, unlike in the case of a screw dislocation (see Section 3.1). For that reason precipitation hardening in the edge case is expected to be slightly dependent on temperature.

In Fig. 9a we show that the critical shape of a dislocation bypassing a row of carbides is similar to that achieved with isotropic dislocation mobility and this result is independent of the carbide spacing. In addition we show in Fig. 9b that the associated strengthening is almost independent of temperature and close to that predicted by the BSK model [30].

The case of non-screw dislocations is then easy to predict and similar to the interaction measured in the athermal regime. This is due to the fact that the screw dipole generated during the bypassing process is of low mobility in comparison with non-screw dislocations. A stress increment is therefore needed to generate the screw dipole bordering the carbides and the elongation of this dipole does not involve a large increase in the stress. When the screw dipole is long enough the mobility of screw dislocation increases sufficiently to enable bypassing of carbides.

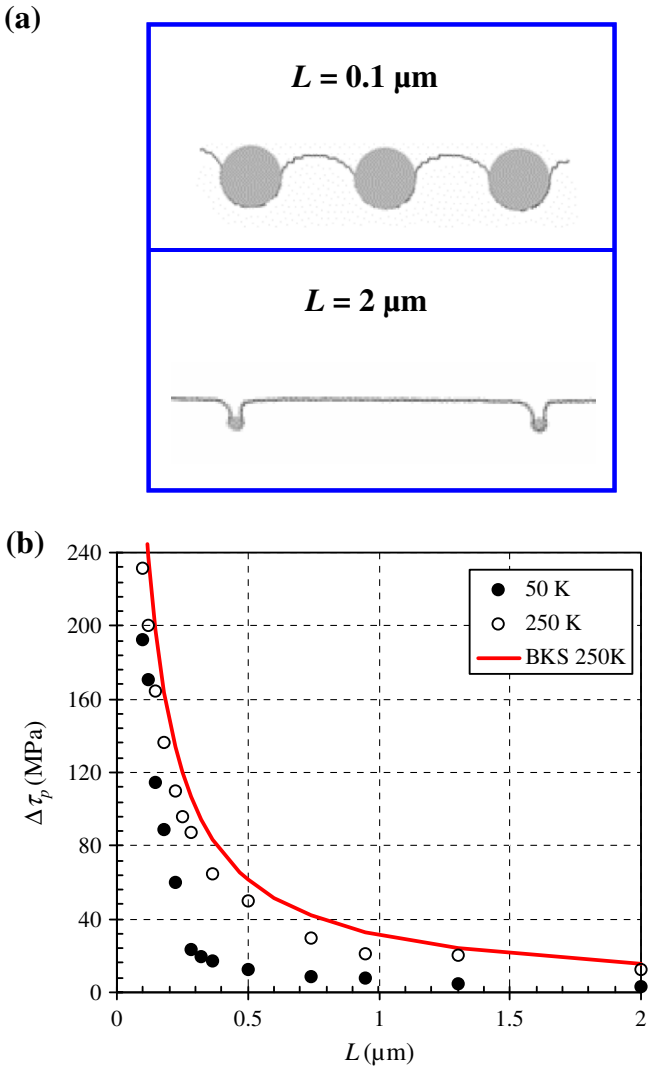

Fig. 10. Critical shape of the screw dislocation at 50 K with different carbide spacing and (b) the Orowan strengthening as a function of carbide spacing for 50 and 250 K. The line recalls the prediction of the BKS model at 250 K.

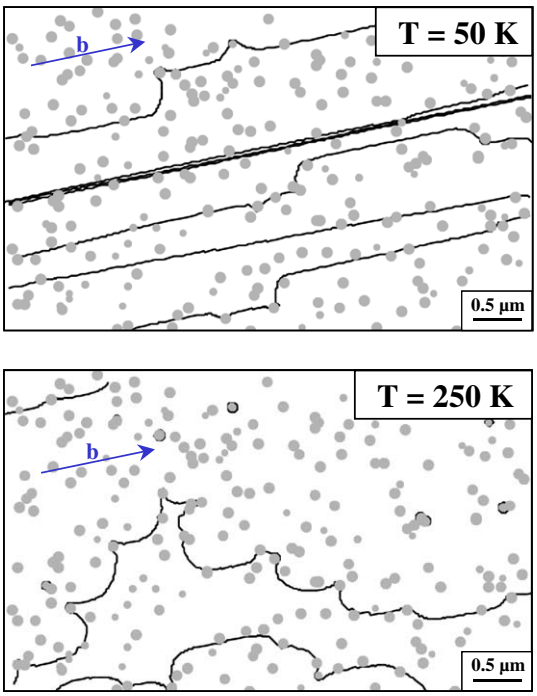

Fig. 11. Comparison between the dislocation microstructure obtained at 50 and 250 K.

4.2.2. Infinite screw dislocation interacting with periodic row of carbides

Unlike the edge segment, the screw segment mobility is strongly dependent on stress and temperature and is affected by the dislocation segment length. DD results clearly show that by decreasing the temperature the strengthening decreases also.

It appears that strengthening follows two regimes: (i) at large precipitate spacing, the strengthening is small and slightly dependent of the spacing and (ii) at small spacing, the strengthening decreases strongly with spacing, as shown in Fig. 10. When the temperature rises, the strengthening approaches that given in the BSK model but remains below it.

4.2.3. Case of dislocations of random character

An infinite dislocation of random character behaves as a mixture of a screw and edge dislocation. However, the corresponding interaction is rather complicated and not introduced here for the sake of brevity. The behavior of dislocation with random character was investigated in the following study when considering their interaction with a random distribution of carbides. Carbides are introduced in the simulated volume following the same procedure used to characterize the carbide strengthening in the athermal regime. Here we recall only that the dislocation mobility is highly anisotropic which alters the behavior of the dislocation microstructure.

The effect of temperature on the evolution of the microstructure is depicted in Fig. 11. The difference in dislocation shape suggests large differences in the mechanical response of the system.

Here we can state some remarks from a qualitative point of view. On the one hand, at high temperature the anisotropy in dislocation mobility is small and the dislocation-line shape looks like that obtained in the athermal regime. The corresponding strengthening is therefore expected to be the same at room temperature. On the other hand, since screw dislocations are almost not curved at low temperature, we suspect the microstructure is not affected by the presence of carbide.

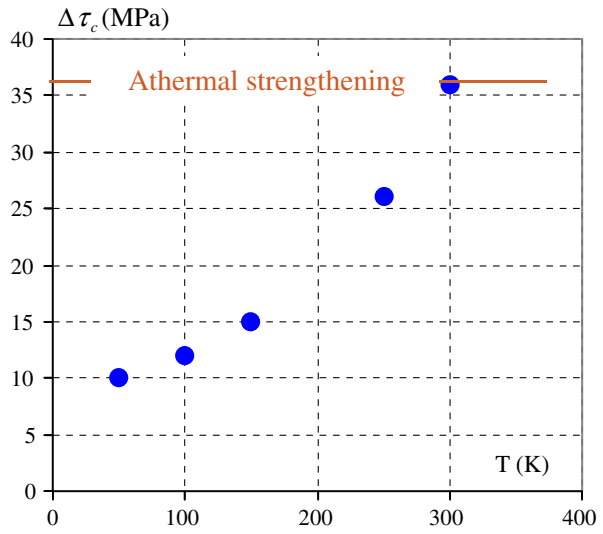

Fig. 12. Carbide induced strengthening in RPV in the athermal regime.

In order to have a more precise prediction of carbide effect on the mechanical response, four similar DD simulations were carried out at different temperatures, as seen in Fig. 12. The athermal strengthening is added for comparison.

From such comparison we can see that carbide strengthening decreases strongly at low temperature. It tends to a threshold of almost 10 MPa at very low temperature. When the temperature increases to 300 K, the mobility of edge dislocations approaches that of screw dislocations. The strengthening reaches therefore the athermal strengthening. An additional increase in temperature is not expected to modify this strengthening.

5. Conclusions

Results obtained in the present study allow us to draw the following remarks and conclusions:

- Two screw dislocation core structures were observed in this work depending on the position of the center of the dislocation core, i.e. whether it is in a "soft" or "hard" triangle.
- The Peierls potential of screw dislocations is characterized by two *stable* positions associated with the "soft" and "hard" configurations.
- The dislocation mobility laws developed for the DD simulations in bainite account correctly for the effect of the temperature and strain rate.
- DD simulations are found to reproduce the dislocation microstructure observed in experiment.
- The values of the slip system interaction coefficients shown in this paper are found to be almost independent of the alloy friction stress of the RPV steel.
- Carbide strengthening determined by DD simulations in the athermal regime is well described by the BKS model. It is of the same order of magnitude as the forest strengthening.
- Carbide strengthening is found to decrease with decreasing temperature. Given the large value of the lattice friction, the effect of carbides on the mechanical properties can be neglected in RPV steel at low temperature.

Acknowledgement

This work was partially funded by the European project PERFECT (No. FI6O-CT-2003-508840).

References

[1] H.D. Solomon, C.J. McMahon Jr., Acta Metall. 19 (1971) 291.
[2] Yu. Osetsky, D.J. Bacon, Model Simul. Mater. Sci. Eng. 11 (2003) 427.
[3] C. Domain, G. Monnet, Phys. Rev. Lett. 95 (2005) 215506.
[4] G. Monnet, D. Terentyev, Acta Mater. 57 (2009) 1416–1426.
[5] G. Kresse, J. Hafner, Phys. Rev. B 49 (1994) 14251.
[6] G. Kresse, J. Furthmüller, Phys. Rev. B 54 (1996) 11169.
[7] G. Kresse, D. Joubert, Phys. Rev. B 59 (1999) 1758.
[8] G.J. Ackland, D.J. Bacon, A.F. Calder, T. Harry, Philos. Mag. A 75 (1997) 713.
[9] S.L. Frederiksen, K.W. Jacobsen, Philos. Mag. A 83 (2003) 365.
[10] M.I. Mendelev, S.W. Han, D.J. Srolovitz, G.J. Ackland, D.Y. Sun, M. Asta, Philos. Mag. 83 (2003) 3977.
[11] S. Ismail-Beigi, T.A. Arias, Phys. Rev. Lett. 84 (2000) 1499.
[12] C. Woodward, S.I. Rao, Phys. Rev. Lett. 88 (2002) 216402.
[13] L. Ventelon, F. Villaime, J. Comput. Aided Mater. Des. 14 (2007) 85.
[14] T. Takeuchi, Trans. Iron Steel Inst. Jpn. 8 (1968) 251.
[15] W.A. Spitzig, A.S. Keh, Acta Metall. 18 (1970) 611.
[16] G. Monnet, B. Devincre, Philos. Mag. 86 (2006) 1555.
[17] U.F. Kocks, A.S. Argon, M.F. Ashby, Prog. Mater. Sci. 19 (1975) 1.
[18] M. Karlik, I. Nedbal, J. Siegl, Mater. Sci. Eng. A 357 (2003) 423.
[19] K. Obrtlik, C. Robertson, B. Marini, J. Nucl. Mater. 342 (2005) 35.
[20] P. Franciosi, M. Berveiller, A. Zaoui, Acta Metall. 28 (1980) 273.
[21] P. Franciosi, Acta Metall. 31 (1983) 1331.
[22] G. Schoeck, R. Frydman, Phys. Status Solidi 53 (1972) 661.
[23] R. Madec, B. Devincre, L.P. Kubin, Phys. Rev. Lett. 89 (2002) 255508.
[24] S. Queyreau, G. Monnet, B. Devincre, Int. J. Plasticity 25 (2009) 361.
[25] R. Madec, L.P. Kubin, CIMTEC Proc. (2004) 671.
[26] W.A. Spitzig, A.S. Keh, Acta Metall. 18 (1970) 1021.
[27] Ph. Pareige, Ph.D. Thesis, Université de Rouen, 1994.
[28] S.R. Ortner, J. Duff, D.W. Beardsmore, Rapport SERCO Assurance SA/EIG/15234/R003, 2003.
[29] G. Monnet, Philos. Mag. 86 (2006) 5927.
[30] D.J. Bacon, U.F. Kocks, R.O. Scattergood, Philos. Mag. 28 (1973) 1241.
[31] S. Naamane, G. Monnet, B. Devincre, Int. J. Plasticity, in press, doi:10.1016/j.ijplas.2009.05.003.